J Sol-Gel Sci Technol (2016) 78:299–306
DOI 10.1007/s10971-015-3949-0

ORIGINAL PAPER: NANO-STRUCTURED MATERIALS (PARTICLES, FIBERS, COLLOIDS, COMPOSITES, ETC.)

Synthesis and photocatalytic activity of TiO_2 nanoparticles prepared by sol–gel method

Raad S. Sabry[1] · Yousif K. Al-Haidarie[2] · Muhsin A. Kudhier[3]

Received: 8 July 2015 / Accepted: 28 December 2015 / Published online: 18 January 2016

Abstract TiO_2 nanoparticles were synthesized via sol–gel method by using $TiCl_4$ ethanol solution as precursor. The effects of gelatinization time and calcination temperature were determined. X-ray diffraction measurements showed that TiO_2 nanoparticles were polycrystalline with anatase phase and transform to rutile phase at high temperatures. The effects of gelatinization time and calcination temperature were examined using atomic force microscopy, field emission scanning electron microscopy, and photoluminescence spectra. Particle size increased from 58 to 89 nm when gelatinization time was increased from 1 to 5 days. Moreover, particle size increased from 58 to 111 nm when calcination temperature was increased from 500 to 900 °C. Photoluminescence intensity decreased when gelatinization time and calcination temperature increased. Photocatalytic properties of TiO_2 nanoparticles were evaluated by photocatalytic degradation of methylene blue (MB) in water under UV light irradiation. The outcomes indicated that TiO_2 nanoparticles exhibited efficient photocatalytic activity of up to 68 % after 180 min as shown by the degradation of MB aqueous solution.

Graphical Abstract

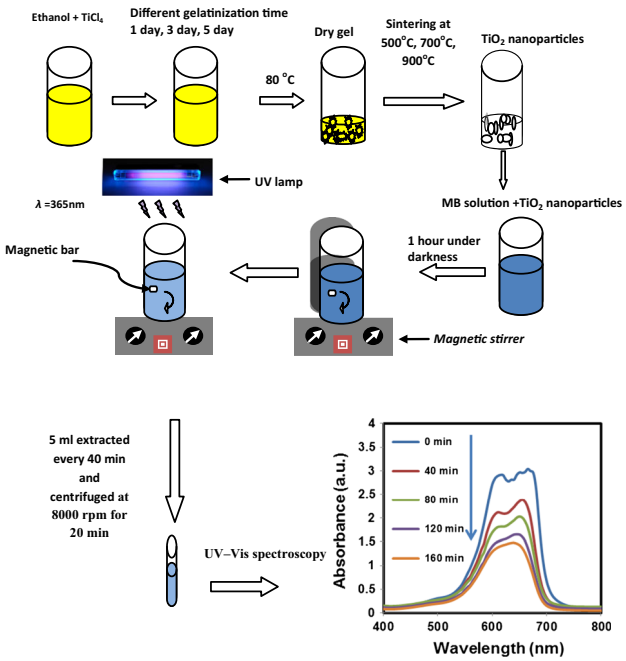

Keywords TiO_2 nanoparticles · Nanostructure · Sol–gel · Photoluminescence spectroscopy

✉ Muhsin A. Kudhier
muhsinattia@yahoo.com

[1] Physics Department, College of Sciences, Al-Mustansiriyah University, Baghdad, Iraq

[2] Chemistry Department, College of Sciences, Al-Mustansiriyah University, Baghdad, Iraq

[3] Physics Department, College of Education, Al-Mustansiriyah University, Baghdad, Iraq

1 Introduction

Titanium dioxide (TiO_2) has recently attracted much attention because of its wide potential applications in environmental remediation, electronics, sensor technology, solar cell, and other related fields [1–6]. TiO_2 offers the most successful application in photocatalysis given its

excellent photoactivity, high-stability, non-toxicity, low-cost, and water-insoluble properties under most conditions. TiO_2 exists in three different crystalline phases, namely rutile (tetragonal), anatase (tetragonal), and brookite (orthorhombic), with each phase providing distinct applications [7–9]. Anatase TiO_2 exhibits higher photocatalytic activity than the other TiO_2 forms [10]. The photocatalytic activity of TiO_2 is influenced by its crystalline form and structural parameters, such as morphology, particle size, and specific surface area [11].

Nanosized TiO_2 is generally prepared by sol–gel method with Ti $(OBU)_4$ as precursor [12, 13]. This process involves expensive chemicals, and the hydrolysis process is not easy to control. There have been many reports of titanium dioxide photocatalysts being successfully prepared using inorganic precursors (such as $TiCl_4$) in the gas phase or the liquid phase [14–17]. In the current study, TiO_2 nanoparticles were synthesized by sol–gel using $TiCl_4$ as precursor because of its low-cost and easy-to-control hydrolysis and quick process. The results confirmed that this process is a good technique to prepare TiO_2 nanoparticles. The mechanisms of gelatinization of $TiCl_4$ ethanol solution and formation of TiO_2 nanoparticles were also determined. Although most of the properties of TiO_2 powder have previously been well studied, photoluminescence (PL) features of TiO_2 powder have not been extensively investigated. Furthermore, PL signals are beneficial to establish the recombination of photoinduced electrons and holes in TiO_2, which can display the behavior of photoinduced electrons and holes. Electrons and holes with distinct behavior exert different effects on photocatalysis. This behavior should be elucidated to analyze the photocatalytic mechanism. In addition, bulk TiO_2 shows no evident PL features compared with the film. Although nanoscaled TiO_2 powder also shows clear PL bands in visible light, PL signals related to the surface structure and oxygen defects are relatively evident, and PL signal corresponding to band-to-band characteristic becomes weak accordingly. Therefore, the PL characteristics of TiO_2 powder should be investigated [18].

Efficient water and air purification technologies based on TiO_2 photocatalysis have been developed. These treatments typically transform toxic organic compounds into non-toxic inorganic compounds. Photocatalytic activity is based on the formation of a photogenerated electron–hole pair upon the absorption of a UV photon. This process involves holes oxidizing the adsorbed organic species and electrons reducing the hydroxyls adsorbed on the surface of OH· radicals. These radicals act as oxidizing agents toward organic species, producing simpler by-products such as CO_2 and H_2O. Thus, organic species deposited on the surface of photocatalysts can be decomposed upon UV irradiation [19].

In this work, the effects of gelatinization time and calcination temperature were examined on the structural and morphological characteristics, crystallite size, and room-temperature PL spectra of anatase TiO_2 nanoparticles. Photocatalytic properties of TiO_2 nanoparticles prepared by sol–gel method were evaluated by photocatalytic degradation of methylene blue (MB) dye in aqueous solution under UV light irradiation at 366 nm. The photocatalytic performance of P25 is also studied and compared with that of synthesized TiO2.

2 Experimental

$TiCl_4$ (>99 %, 1.5 ml; BDH Laboratory Supplies, England) was slowly added dropwise into 15 ml of ethanol (>99 %; Scharlau, Spain). The reaction was performed at room temperature (25 °C) while stirring under a fumehood because of the large amount of Cl_2 and HCl gases evolved from this reaction. A light yellow solution was obtained and gelatinized from 1 to 5 days to form a sol–gel. The final sol–gel solution was then dried at 80 °C, and a dry gel was obtained. Eventually, the dry gel was calcined at 500 °C for 1 h in air to form TiO_2 nanoparticles. The decomposition of organic components in the precursor was promoted by maintaining the initial heating rate at 5 °C/min. The dependence of crystallite size on calcination temperature was investigated. The dry gel, which was gelatinized for 1 day, was also calcined at different calcination temperatures (500, 700, and 900 °C). TiO_2 nanoparticles were examined by powder X-ray diffraction using CuKα (Miniflex II Rigaku, Japan).

TiO_2 powder was deposited onto the glass substrate via screen-printing method. Surface morphology was studied using atomic force microscopy (AFM) (Inc. "Nanoscope III and Dimension 3100"). Samples were observed under a Hitachi S-4160 field emission scanning electron microscope after the samples were coated with gold. Optical absorption spectra of the TiO_2 film were recorded using UV–visible spectrophotometer (Shimadzu UV-1601). PL spectra were recorded at room temperature (25 °C) with a PL spectrophotometer (Shimadzu) by exciting the samples at 260 and 360 nm. Finally, the catalytic activity of the calcined powder was detected by a UV–Vis spectrophotometer.

The photocatalytic activity of the calcined powder was investigated by the degradation of a standard MB solution in a photochemical reactor. A 20 mg/L MB aqueous solution, which was prepared using distilled water, was employed as model pollutant to measure the photocatalytic activity of the TiO_2 catalysts. Approximately 20 mg of TiO_2 photocatalytic powder, which was gelatinized for 1 day and calcined at 500 °C, was added into a quartz

beaker containing 50 mL of MB aqueous solution. The solution was placed in a photocatalytic reactor and stirred in the dark for 60 min to ensure the establishment of adsorption and desorption equilibrium of MB on the TiO_2 surface. The suspension was subsequently irradiated with a UV lamp ($\lambda = 366$ nm; CAMAG company). The suspension was gently stirred throughout the experiment to maintain its stability. At 40-min interval, 5 mL of the suspension was extracted and then centrifuged at 8000 rev/min for 20 min to separate the powder from the supernatant. UV–Vis spectroscopy was used to generate time-dependent absorbance changes in the supernatant between 400 and 800 nm. Color removal of the dye solution was determined by measuring the absorbance at $\lambda = 664$ nm with a UV–visible spectrophotometer, which was initially calibrated in accordance with Beer–Lambert's law. The same experimental procedure was followed for Degussa P25 powder obtained from (Nippon Aerosil Co., Ltd) to compare with the synthesized one.

3 Results and discussion

Figure 1 shows the XRD patterns of TiO_2 powders prepared at different gelatinization times and calcined at 500 °C for 1 h in air. The peaks in the XRD patterns correspond to the (101), (112), (200), (105), (211), (204), (116), (220), and (215) planes of the TiO_2 tetragonal anatase phase. Crystallite sizes were calculated using Scherrer formula [20]:

$$D = \frac{k\lambda}{\beta \cos\theta} \quad (1)$$

where D is the crystallite size in nanometers, k is a constant (0.9, assuming that the particles are spherical), λ is the wavelength of the X-ray radiation (CuK$\alpha = 0.1541$ nm), β is the FWHM (full width at half maximum) of the strongest peak, and θ is the diffraction angle. The crystallite sizes of the powders were calculated using the diffraction peaks of the anatase (101) crystalline plane. The results showed that the crystallite sizes of the samples were 13.85, 15.05, and 16.49 nm for the powders gelatinized within 1, 3, and 5 days, respectively. No peak for the brookite or rutile phase was detected, indicating high purity of the as-prepared samples. These findings revealed that the resultant powders were all in TiO_2 anatase phase. Figure 2 shows the XRD patterns of powders prepared in 1 day of gelatinization time and calcined at different temperatures, the powder calcined at 700 °C clearly confirms the coexistence of anatase and rutile. As can be seen in Fig. 2b, the 2θ values at 25.28, 38.52, and 48.05° can be assigned to (101), (112), and (200) crystal planes of anatase TiO_2. And 27.4, 36.20, 41.26, and 54.36° can be assigned to (110), (101), (111), and (211) crystal planes of rutile TiO_2. All peaks can be indexed to anatase (JCPDS card No. 21-1272) and rutile (JCPDS card No. 1276). The mass percent of anatase in the product is 52 % and rutile is 48 % which was obtained from the equation [21]:

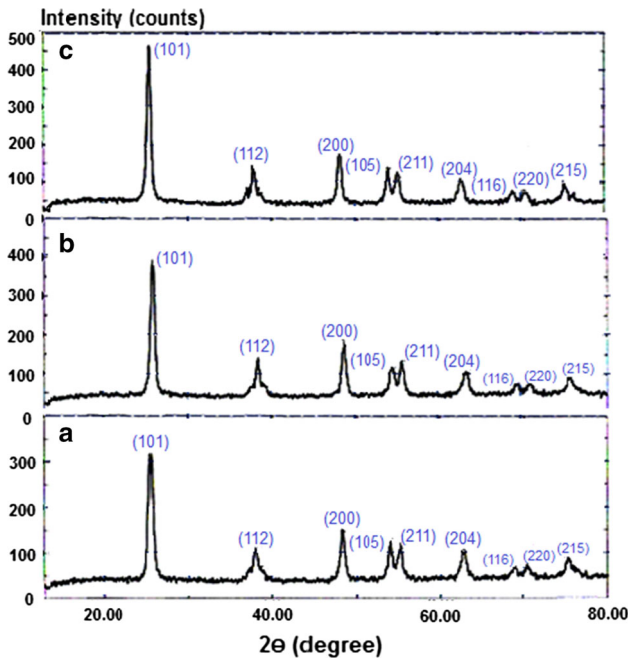

Fig. 1 XRD spectra of anatase TiO_2 powder for different gelatinization times *a* 1 day, *b* 3 days, *c* 5 days

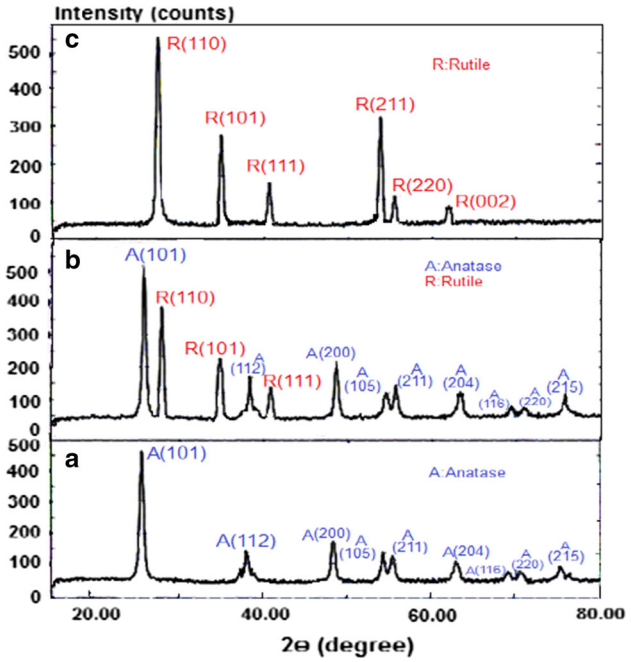

Fig. 2 XRD spectra of TiO_2 powder for different calcination temperatures *a* 500 °C, *b* 700 °C, *c* 900 °C

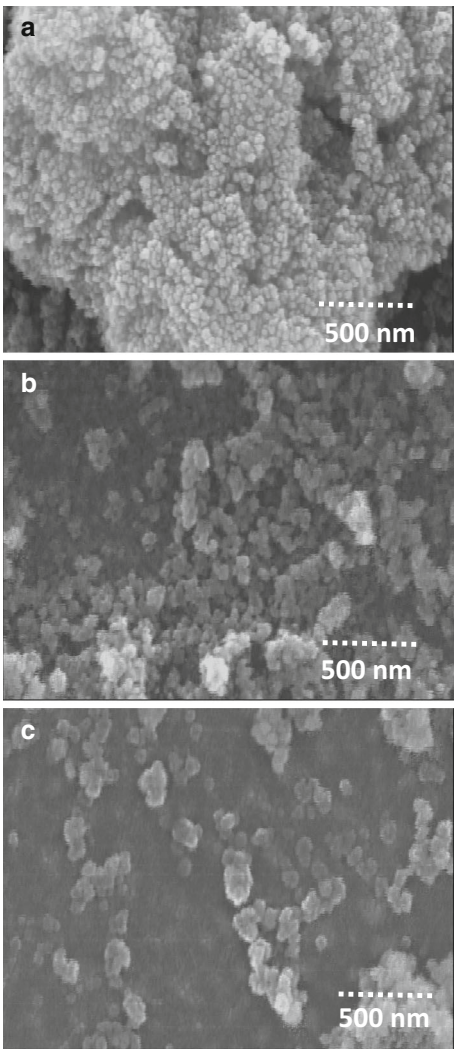

Fig. 3 FESEM images of TiO_2 films with different gelatinization times **a** 1 day, **b** 3 days, **c** 5 days

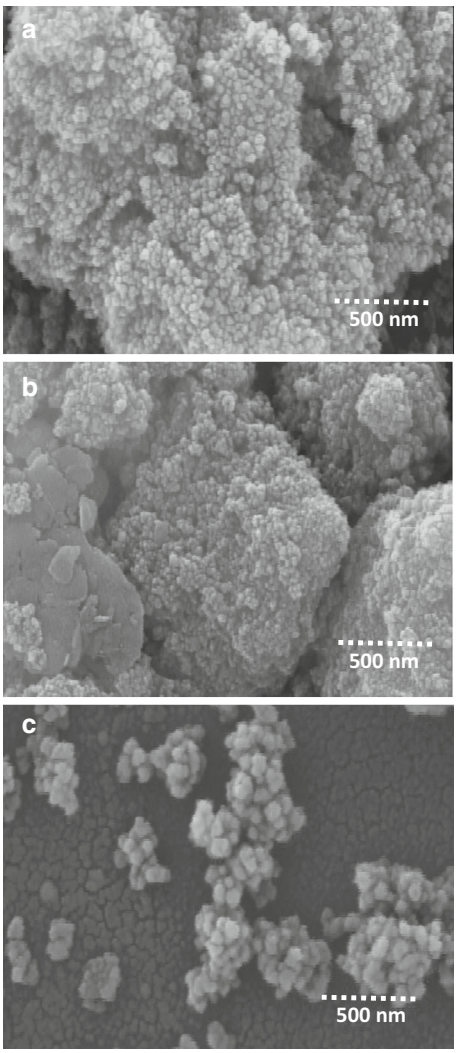

Fig. 4 FESEM images of TiO_2 films gelatinized for 1 day with different calcination temperatures **a** 500 °C, **b** 700 °C, **c** 900 °C

$$m_A = \frac{1}{\left[1 + 1.26\left(\frac{I_R}{I_A}\right)\right]} \tag{2}$$

where m_A is the mass fraction of anatase in the mixture and I_A and I_R were obtained from the peak areas of anatase (101) and rutile (110) diffraction peaks, respectively. The powder calcined at 900 °C shows the existence of rutile phase only. The crystallite sizes were 13.85, 16.20, and 17.75 nm for the powders calcined at 500, 700, and 900 °C, respectively.

The lattice constants of TiO_2 nanoparticles were calculated using the following equation [22]:

$$\frac{1}{d^2} = \frac{h^2 + k^2}{a^2} + \frac{l^2}{c^2} \tag{3}$$

where d is the interplanar distance, and h, k, and l are the Miller indices. Moreover, a and c are the lattice constants for the tetragonal structure. The anatase lattice constants were $a = 0.378$ nm and $c = 0.\ 954$ nm, while the rutile lattice constants were $a = 0.460$ nm and $c = 0.296$ nm, which are in good agreement with JCPDS card No. 21-1272 ($a = 0.\ 379$ nm and $c = 0.\ 951$ nm) and JCPDS card No. 21-1276 ($a = 0.459$ nm and $c = 0.296$) for anatase and rutile phases, respectively. Increasing the gelatinization time and calcination temperature resulted in larger crystallites sizes of the powders because of the hydrolysis and polymerization of the precursor.

Surface morphology and roughness are indicated in the AFM images in Figs. 3 and 4. The average roughness values were 65.25, 82.10, and 88.31 nm for the powders prepared with gelatinization times of 1, 3, and 5 days, respectively. By contrast, the average roughness values were 65.25, 96.69, and 101.17 nm for the powders calcined at 500, 700, and 900 °C, respectively.

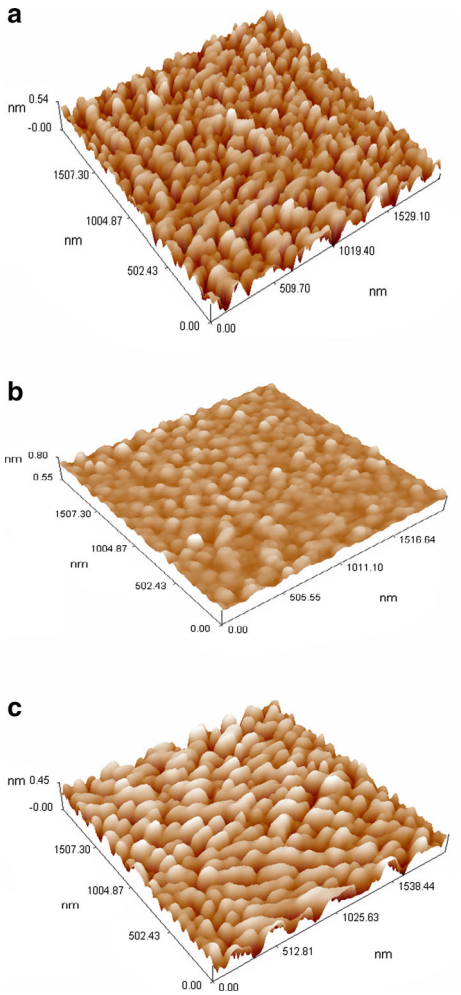

Fig. 5 AFM images of TiO_2 films for different gelatinization times **a** 1 day, **b** 3 days, **c** 5 days

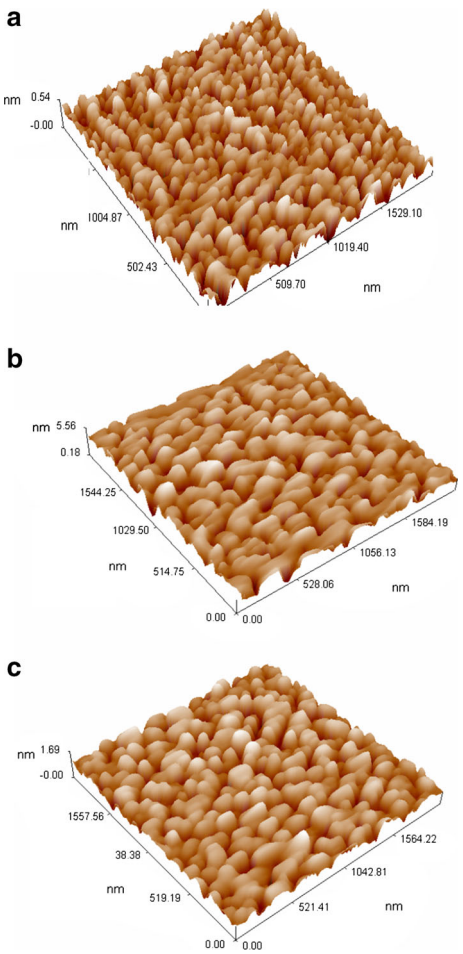

Fig. 6 AFM images of TiO_2 films for different calcination temperatures **a** 500 °C, **b** 700 °C, **c** 900 °C

Figures 5 and 6 present the scanning electron micrographs of TiO_2 nanoparticles synthesized in terms of different experimental conditions. These micrographs reveal that the shape of the particles was influenced by the experimental conditions. Scanning electron micrographs of the nanostructures of all samples were analyzed by Image Processing analytical software to obtain the average grain size of the samples. The grain size increased from 58 to 89 nm with gelatinization time increased from 1 to 5 days. Increasing the gelatinizing time improved the dispersivity and increased the grain size [23]. The grain size increased from 58 to 111 nm with calcination temperature increased from 500 to 900 °C. As the calcination temperature increased, the particles agglomerated, resulting in increased grain size.

PL spectroscopy is a practical method for probing the electronic structure of nanomaterials, the transfer behavior of photoexcited electron–hole pairs in semiconductors, and the rate of recombination [24]. PL emission spectra have been widely used to investigate the efficiency of charge carrier trapping and migration and understand the fate of electron–hole pairs in semiconductors [25]. Figure 7 shows the PL spectra of TiO_2 nanoparticles recorded at room temperature and excitation wavelength of 260 nm. Two groups of peaks were observed. The first peaks at 359, 374, and 385 nm can be ascribed to the emission of band gap transition related to the anatase structure of TiO_2 [26], whereas the second emission band at 454, 471, 485, and 496 nm originated from the charge recombination at the shallow-trap surface state [27]. These surface states originated from the oxygen vacancies, which acted as radiative centers. These defect states play an important role in determining the reflective properties and photocatalytic properties of TiO_2 nanoparticles [28].

Figure 8 shows the PL spectra at the excitation wavelength of 360 nm. Several peaks at 396, 425, 454, 471, 486, and 496 nm were observed. The first emission peak was

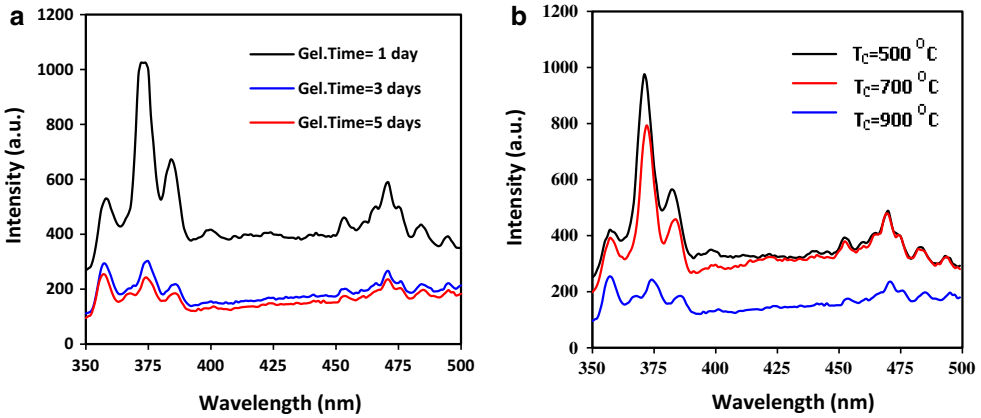

Fig. 7 PL spectra of TiO_2 films at excitation wavelength of 260 nm for different **a** gelatinization times and **b** calcination temperatures

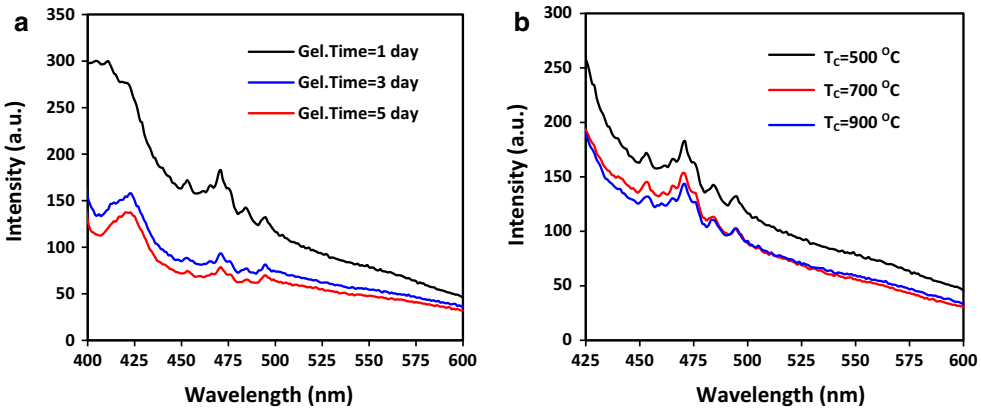

Fig. 8 PL spectra of TiO_2 films at excitation wavelength of 360 nm for different **a** gelatinization times and **b** calcination temperatures

ascribed to the annihilation of excitons, whereas the remaining five peaks were from the surface states. The emission peaks in the visible region were attributed to the defect levels below the conduction band. The native defects in the wide gap semiconductors were expected to introduce deep levels inside the band gap. The broad luminescence spectrum in the visible region is attributed to the electronic transition mediated by the defect levels, such as oxygen vacancies in the band gap [29]. As the number of oxygen vacancies and defects increased, the PL intensity also increased [30].

The PL emission mainly results from the recombination of excited electrons and holes, and the lower PL intensity indicates the decrease in recombination rate [31]. The decreases in the PL intensity with gelatinization time and calcination temperature belong to increase in the grain size and decrease in dislocation levels with these parameters as mentioned previously in SEM results.

The UV–Vis spectral change of 20 mg/L MB as a function of irradiation time during the photodegradation by TiO_2 nanoparticle photocatalysts is shown in Fig. 9. The powder gelatinized for 1 day and calcined at 500 °C was selected as the photocatalyst to determine the photocatalytic activity of the TiO_2 nanoparticles. When irradiation time was increased from 0 to 180 min, the intensity of the characteristic absorption band at the 664 nm peak decreased gradually, suggesting that MB was gradually photodegraded by the TiO_2 nanoparticle photocatalysts. A large amount of MB was removed from the solution after 180 min of degradation.

When TiO_2 is illuminated by UV light, electrons are excited from the valence band to the conduction band, thereby generating electron–hole pairs [32]. The holes in TiO_2 react with water molecules or hydroxide ions, hence producing hydroxyl radicals. Oxygen is usually supplied as an electron acceptor to prolong the recombination of electron–hole pairs during photocatalytic oxidation. The hydroxyl radical is a powerful oxidizing agent that attacks organic pollutants present at or near the surface of TiO_2 [33]. This process results in the photooxidation of

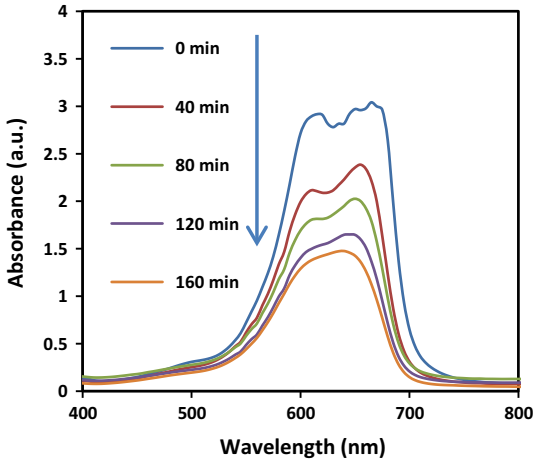

Fig. 9 UV–vis absorption spectra of photocatalytic degradation of MB recorded at different time intervals by the TiO_2 photocatalys

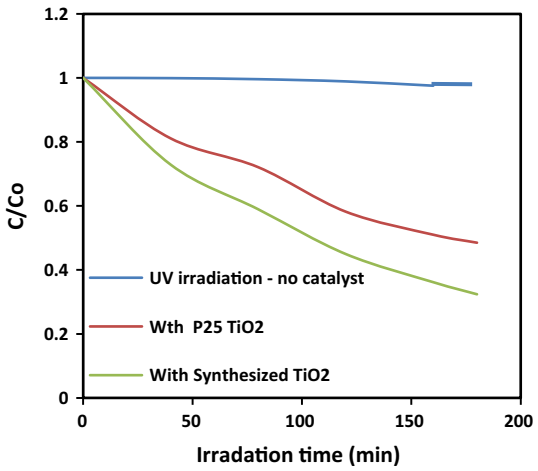

Fig. 10 Time-dependent photodegradation of MB under UV irradiation with and without synthesized and P25 TiO_2 photocatalyst

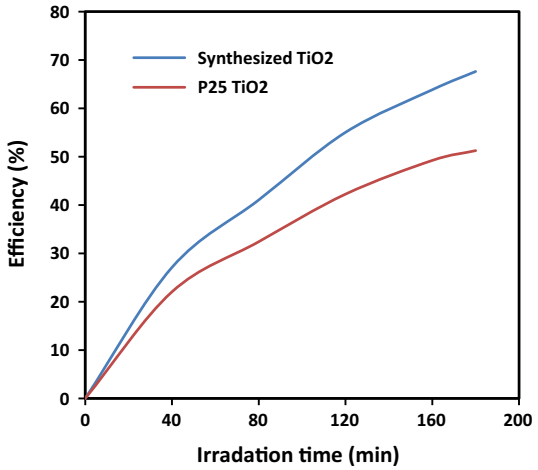

Fig. 11 Degradation efficiency of MB using synthesized and P25 TiO_2 photocatalyst

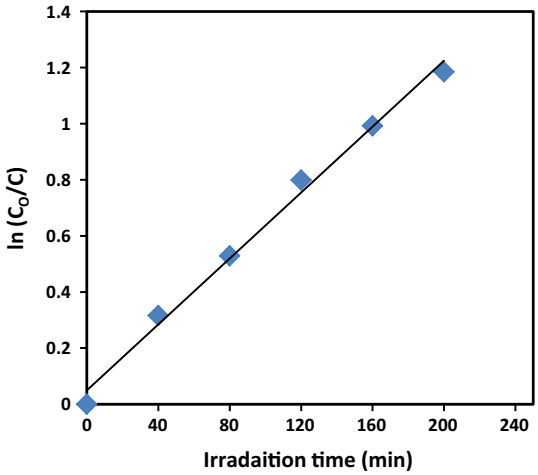

Fig. 12 First-order kinetics of the degradation of (MB) dye with irradiation time

pollutants, in accordance with the following processes: (i) photon absorption of the semiconductor catalyst, (ii) generation of electrons and holes, (iii) transfer of charge carriers, and (iv) utilization of charge carriers by the reactants.

Time-dependent photodegradation of MB is illustrated in Fig. 10. MB decomposed in the synthesized and P25 TiO_2 under UV light irradiation. The photodegradation efficiency for each experiment, also called conversion, was estimated by the following relationship [34] and is shown in Fig. 11:

$$X(\%) = \frac{C_0 - C}{C_0} \times 100\% \quad (4)$$

where X is the photodegradation efficiency, C_0 is the concentration of MB before illumination, and C is the concentration of MB in the suspension after time t (mg/L). The pseudo first-order rate constant k (min^{-1}) can be calculated using the slope of the line from Fig. 12. The value of k was 0.006 min^{-1}, and the efficiency after 180 min was 68 %; for the synthesized TiO_2 nanoparticles, this value is higher than that of P25 which is 51 %.

4 Conclusions

Anatase TiO_2 nanoparticles were successfully synthesized via sol–gel method with $TiCl_4$ as precursor. This low-cost and easy-fabrication method can be performed at room temperature. XRD results showed that crystallite size increases when gelatinization time and calcination temperature are increased. By contrast, PL intensity decreases with increasing gelatinization time and calcination

temperature. The degradation efficiency to MB by synthesized titania is larger than that of P25 TiO_2. Overall, the improved efficiency through the photocatalytic process is attributed to the large specific surface area of the TiO_2 nanoparticles.

References

1. Chen X, Mao SS (2007) Titanium dioxide nanomaterials: synthesis, properties, modifications, and applications. Chem Rev 107(7):2891
2. Lee S, Cho IS, Lee JH, Hoe Kim D, Wook Kim D, Young Kim J, Shin H, Lee J, Jung H, Park N, Kim K, Jae Ko M, Hong K (2010) Two-step sol–gel method-based TiO_2 nanoparticles with uniform morphology and size for efficient photo-energy conversion devices. Chem Mater 22(6):1958
3. Yang D, Liu H, Zheng Z, Yuan Y, Zhao J, Waclawik E, Ke X, Zhu H (2009) An efficient photocatalyst structure: TiO_2(-B) nanofibers with a shell of anatase nanocrystals. J Am Chem Soc 131(49):17885
4. Choi SK, Kim S, Lim SK, Park H (2010) Photocatalytic comparison of TiO_2 nanoparticles and electrospun TiO_2 nanofibers: effects of mesoporosity and interparticle charge transfer. J Phys Chem C 114(39):16475
5. Chuangchote S, Jitputti J, Sagawa T, Yoshikawa S (2009) Photocatalytic activity for hydrogen evolution of electrospun TiO_2 nanofibers. ACS Appl Mater Interfaces 1(5):1140
6. Song MY, Kim DK, Ihn KJ, Jo SM, Kim DY (2004) Electrospun TiO_2 electrodes for dye-sensitized solar cells. Nanotechnology 15(12):1861
7. Fujishima A, Honda K (1972) Electrochemical photolysis of water at a semiconductor electrode. Nature 283:37
8. Diebold U (2003) The surface science of titanium dioxide. Surf Sci Rep 28:53
9. Carp O, Huisman CL, Reller A (2004) Photoinduced reactivity of titanium dioxide. Solid State Chem 32:33
10. Sclafani A, Palmisano L, Schiavello M (1990) Influence of the preparation methods of titanium dioxide on the photocatalytic degradation of phenol in aqueous dispersion. J Phys Chem 94(2):829
11. Yu J, Wang G, Cheng B, Zhou M (2007) Effects of hydrothermal temperature and time on the photocatalytic activity and microstructures of bimodal mesoporous TiO_2 powders. Appl Catal B Environ 69:171
12. Kresge CT, Leonowica ME, Roth WJ, Vartuli JC, Beck JS (1992) Ordered mesoporous molecular sieves synthesized by a liquid-crystal template mechanism. Nature 359:710
13. Barbe CJ, Arendse F, Comte P, Jirousek M, Lenzmann F, Shklover V, Gratzel M (1997) Nanocrystalline titanium oxide electrodes for photovoltaic applications. Am Ceram Soc 80(12):3157
14. Bessekhouad Y, Robert D, Weber JV (2003) Preparation of TiO_2 nanoparticles by Sol–Gel route. Int J Photoenergy 5:153
15. Gholami M, Bahar M, Azim-Araghi ME (2012) The preparation of TiO_2 nanoparticles and investigation of its electrical properties as CO2 gas sensor at room temperature. Elixir Chem Phys Lett 48:9626
16. Haghighi F, Roudbar Mohammadi S, Mohammadi P, Hosseinkhani S, Shidpour R (2013) Antifungal activity of TiO_2 nanoparticles and EDTA on Candida albicans Biofilm. Infect Epidemiol Med 1(1):33
17. Li W, Zeng T (2011) Preparation of TiO_2 anatase nanocrystals by TiCl4 hydrolysis with additive H2SO4. PLoS ONE 6(6):e21082
18. Liu B, Wen L, Zhao X (2007) The photoluminescence spectroscopic study of anatase TiO_2 prepared by magnetron sputtering. Mater Chem Phys 106:350
19. Abellan MN, Dillert R, Gimenez J, Bahnemann D (2009) Evaluation of two types of TiO_2-based catalysts by photodegradation of DMSO in aqueous suspension. J Photochem Photobiol A Chem 202:164
20. Warren BE (1990) X-ray diffraction. Dover, New York
21. Spurr RA, Myers H (1957) Quantitative analysis of anatase- rutile mixtures with an X-ray diffractometer. Anal Chem 29(5):760
22. Ladd MFC, Palmer RA (1993) Structure determination by X-ray crystallography, 3rd edn. Plenum Press, New York
23. Sugapriya S, Sriram R, Lakshmi S (2013) Effect of annealing on TiO_2 nanoparticles, Optik- Inter. J Light Electron Opt 24:4971
24. Hurum DC, Agrios AG, Gray KA, Rajh T, Thurnauer MC (2003) Explaining the enhanced photocatalytic activity of degussa P25 mixed-phase TiO_2 using EPR. J. Phys. Chem. B 107:4545
25. Cong Y, Zhang J, Chen F, Anpo M, He D (2007) Preparation, photocatalytic activity, and mechanism of nano-TiO_2 Co-doped with nitrogen and iron (III). J Phys Chem C 111(28):10618
26. Yu JC, Yu JG, Ho WK, Zhang LZ (2002) Effects of F- doping on the photocatalytic activity and microstructures of nanocrystalline TiO_2 powders. Chem Mater 14:3808
27. Yoon M, Seo M, Jeong C, Jang JH, Jeon KS (2005) Synthesis of liposome-templated titania nanodisks: optical properties and photocatalytic activities. Chem Mater 17(24):6069
28. Ullmann F (2002) Encyclopedia of industrial chemistry. Wiley, Weinheim
29. Behera D, Bag B, Sakthivel R (2011) Synthesis, characterization and photoluminescence study of modified titania. Indian J Pure Appl Phys 49:754
30. Xiao Q, Si Z, Yu Z, Qiu G (2007) Sol–gel auto-combustion synthesis of samarium-doped TiO_2 nanoparticles and their photocatalytic activity under visible light irradiation. Mater Sci Eng B 137:189
31. Li XZ, Li FB, Yang CL, Ge KW (2001) Photocatalytic activity of WOx-TiO_2 under visible light irradiation. J Photochem Photobiol A 141:209
32. Lao JY, Wen JG, Ren ZF (2002) Hierarchical ZnO nanostructures. Nano Lett 11:1287
33. Wang ZL, Pan ZW (2002) Junctions and networks of SnO nanoribbons. Adv Mater 14:1029
34. Mengyue Z, Shifu C, Yaowu T (1995) Photocatalytic degradation of organophosphorus pesticides using thin films of TiO_2. J Chem Tech Biotechno 64:339